Electric Nondipole Effect in Strong-Field Ionization

A. Hartung,[1] S. Brennecke,[2] K. Lin,[1,3,*] D. Trabert,[1] K. Fehre,[1] J. Rist,[1] M. S. Schöffler,[1] T. Jahnke,[1] L. Ph. H. Schmidt,[1] M. Kunitski,[1] M. Lein,[2] R. Dörner,[1,†] and S. Eckart[1,‡]
[1]*Institut für Kernphysik, Goethe-Universität, Max-von-Laue-Straße 1, 60438 Frankfurt, Germany*
[2]*Institut für Theoretische Physik, Leibniz Universität Hannover, Appelstraße 2, 30167 Hannover, Germany*
[3]*State Key Laboratory of Precision Spectroscopy, East China Normal University, 200241, Shanghai, China*

(Received 17 August 2020; accepted 8 January 2021; published 4 February 2021)

Strong-field ionization of atoms by circularly polarized femtosecond laser pulses produces a donut-shaped electron momentum distribution. Within the dipole approximation this distribution is symmetric with respect to the polarization plane. The magnetic component of the light field is known to shift this distribution forward. Here, we show that this *magnetic* nondipole effect is not the only nondipole effect in strong-field ionization. We find that an *electric* nondipole effect arises that is due to the position dependence of the electric field and which can be understood in analogy to the Doppler effect. This *electric* nondipole effect manifests as an increase of the radius of the donut-shaped photoelectron momentum distribution for forward-directed momenta and as a decrease of this radius for backwards-directed electrons. We present experimental data showing this fingerprint of the *electric* nondipole effect and compare our findings with a classical model and quantum calculations.

DOI: 10.1103/PhysRevLett.126.053202

The ionization of an atom by the interaction with an electromagnetic wave is often described by only considering the temporal evolution of the electric field vector. This is at the heart of the dipole approximation which neglects the magnetic component and the position dependence of the light field. It is a surprisingly good approximation over a wide range of wavelengths and intensities from the perturbative single-photon ionization regime of the photoelectric effect over multiphoton ionization to strong-field nonrelativistic tunnel ionization. Single-photon ionization is dominated by electric dipole transitions [1,2]. The same holds in the nonrelativistic strong-field regime where it is the time-dependent *electric* field that drives tunnel ionization and determines the electron momentum distribution in a good approximation [3,4]. Within the dipole approximation, the momentum distribution of the emitted electrons is forward-backward symmetric for single-photon ionization [5] as well as for strong-field ionization [6].

The leading physical mechanisms which eventually lead to a failure of the dipole approximation and a breaking of the forward-backward symmetry of electron emission are different for single-photon and strong-field ionization. For single-photon ionization the dominating term beyond electric dipole transitions is due to electric quadrupole transitions. The interference between electric dipole and electric quadrupole transitions leads to a breaking of the symmetry and at high photon energies to a forward emission of photoelectrons and backward emission of ions [2,7–10]. The electric quadrupole transitions are due to the spatial dependence of the electric field whereas the transition amplitudes that are driven by the magnetic component of the field are typically much weaker [2]. In contrast, for strong-field ionization the breakdown of the dipole approximation [4,11–15] is commonly argued to be due to the magnetic component of the light field that drives the electron forward via the Lorentz force [16] (for the effect of rescattering see Refs. [17–20]). However, the temporospatial dependence of the electric field has not been discussed so far for strong-field ionization at nonrelativistic intensities. Up to now, no experimental evidence has been presented which shows an influence of the temporospatial nature of the light field in strong-field ionization that breaks the forward-backward symmetry. It is the purpose of the present Letter to provide that missing experimental evidence and show how the temporospatial dependence of the electric field alters electron momentum distributions in strong-field ionization. We show that electric field driven nondipole effects are as important as those caused by the magnetic field, if a suitable observable is looked at.

We consider circularly polarized light, to avoid the additional complexity caused by recollisions of the electron with its parent ion. Upon ionization of an atom by a circularly polarized, multicycle laser pulse at a wavelength of 800 nm the electron momentum distribution has a donutlike shape [blue shape in Fig. 1(a)]. The radius of the donut in momentum space is approximately given by

$$\langle p_r \rangle = A_0 = \frac{E}{\omega}, \tag{1}$$

where $p_r = \sqrt{p_y^2 + p_z^2}$ is the radial momentum component perpendicular to the light propagation direction, E is the

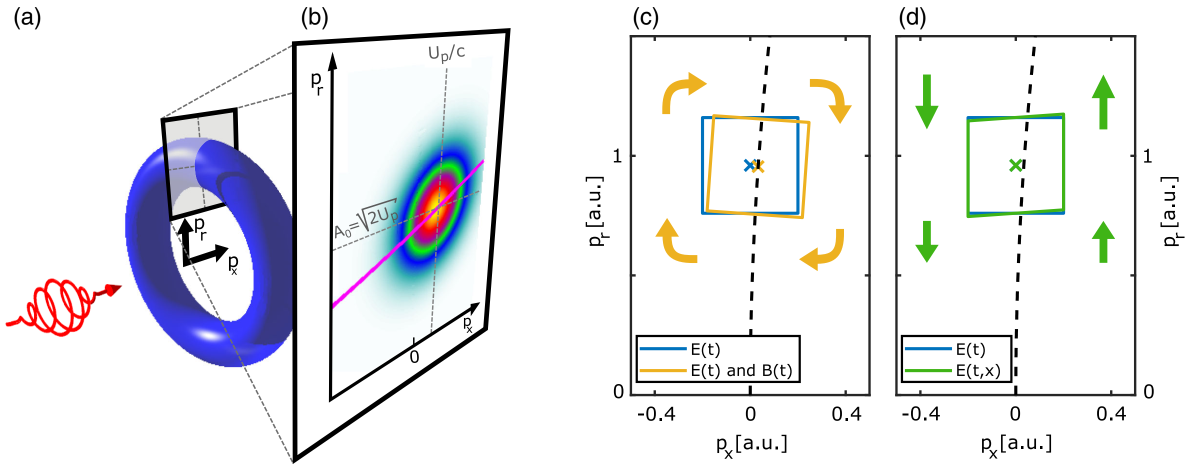

FIG. 1. (a) Illustration of the donut shape of the electron momentum distribution from strong-field ionization in a circularly polarized laser pulse and of the coordinate system that is used throughout our Letter. (b) Artist's view of a combination of the two nondipole effects. The *magnetic* component of the light field drives the donut forward by about U_p/c through the magnetic part of the Lorentz force. The temporospatial *electric* field results in an increase of $\langle p_r \rangle$ as a function of p_x [purple line in (b)]. (c) Four classical trajectories are calculated using the dipole approximation. The initial momenta after tunneling are chosen such that the final electron momenta mark the edges of the blue square. Using the same initial conditions but including the magnetic component only (no spatial dependence of the electric field) leads to the yellow quadrangle in (c) which is forward shifted and rotated with respect to the blue square. For the green quadrangle in (d) the temporospatial electric field is considered and the magnetic field is neglected which leads to shearing of the electron momentum distribution as indicated. In (c) and (d) the crosses indicate the centers of the quadrangles and the dashed lines correspond to the naively expected forward shift of $0.5p_r^2/c$. For visual representation, both effects are amplified by a factor of 10 (see text).

laser's peak electric field, ω is the central frequency of the laser pulse, and A_0 is the laser's peak vector potential (atomic units are used unless stated otherwise). When calculated within the dipole approximation, this donut is symmetric with respect to the polarization plane ($p_y p_z$ plane). In pioneering work Smeenk *et al.* showed experimentally that this momentum distribution is slightly forward shifted by about U_p/c [11] ($U_p = (E^2/2\omega^2)$ is the ponderomotive energy and U_p/c is the forward momentum which classical mechanics predicts for an electron launched with zero initial velocity and accelerated by a circularly polarized *spatially homogeneous* electromagnetic field.) Soon after, Klaiber *et al.* [21] predicted an additional forward shift of $I_p/(3c)$ (with the ionization potential I_p) which was confirmed by other calculations [12,22,23] and an experiment [24]. In all cases, these forward shifts were discussed to be due to the magnetic component of the light field.

Figure 1(b) shows an artist's view of the full nondipole effect in strong-field ionization (including the magnetic and the electric nondipole effect) in cylindrical coordinates (p_x, p_r). To further investigate these nondipole effects, we use classical trajectory simulations (CTSs) consisting of two steps. In the first step the electron is freed by laser-induced tunnel ionization. In a second step the electron's acceleration in the time- and position-dependent electromagnetic field is described classically by Newton's equation. For this second step the Coulomb interaction of the electron and its parent ion are not taken into account [25]. The CTS model is well suited to distinguish electric and magnetic field driven nondipole effects. We assume adiabatic tunneling, i.e., that after tunneling the electrons have zero initial velocity in tunnel direction and their velocity in both directions perpendicular to the tunnel direction is described by a rotationally symmetric initial Gaussian momentum distribution that is centered at zero momentum (analogous to Eq. (9) of Ref. [26]). The electric and magnetic field of the circularly polarized laser pulse are defined by

$$\vec{E}(x,t) = E_0(t)\begin{pmatrix} 0 \\ \cos\left(\omega t - \zeta \frac{\omega}{c} x\right) \\ \sin\left(\omega t - \zeta \frac{\omega}{c} x\right) \end{pmatrix},$$

$$\vec{B}(x,t) = \chi \frac{E_0(t)}{c}\begin{pmatrix} 0 \\ -\sin\left(\omega t - \zeta \frac{\omega}{c} x\right) \\ \cos\left(\omega t - \zeta \frac{\omega}{c} x\right) \end{pmatrix}. \quad (2)$$

Here, $E_0(t)$ is the temporal envelope of the light pulse. For a real light pulse one sets $\zeta = \chi = 1$ while in the dipole approximation one sets $\zeta = \chi = 0$.

Taking only the magnetic field into account ($\zeta = 0$, $\chi = 1$) leads to the well-known forward shift of the donut-shaped electron momentum distribution by U_p/c [11] and an additional internal rotation of the electron momentum distribution around its center by an angle of about A_0/c as schematically illustrated in Fig. 1(c). Importantly, the most probable radial momentum $\langle p_r \rangle$ of the distribution as a function of p_x remains constant in this case.

In full analogy, the effect of the temporospatial dependence of the electric field $\vec{E}(x,t)$ alone ($\zeta = 1, \chi = 0$) can be included in the calculations. The temporospatial electric field $\vec{E}(x,t)$ leads to a shearing of the final momentum distribution as compared to an electric field $\vec{E}(t)$ that is only time dependent [see Fig. 1(d)].

Strikingly, the increase of the radius of the donut-shaped electron momentum distribution as a function of p_x, which is shown in Fig. 1(b) from an artist's perspective, can be interpreted in analogy to the Doppler effect. In the lab frame, electrons that propagate parallel (antiparallel) to the light-propagation direction experience an oscillating force with a frequency that is lower (higher) than the central frequency of the incident laser field. The frequency of this oscillating force is given by $\bar{\omega}(p_x) = \omega(1 - p_x/c)$ for a light propagation direction that is parallel to p_x. Using this insight one can approximate the most probable radial electron momentum $\langle p_r \rangle$ for a given value of p_x. To this end Eq. (1) is generalized using $\bar{\omega}(p_x)$ instead of ω which leads to

$$\langle p_r \rangle(p_x) = \frac{E}{\bar{\omega}(p_x)} \approx \left(1 + \alpha \frac{p_x}{c}\right) A_0 \qquad (3)$$

where $\alpha = 1$ in this simplest case. Later, we will use α as a fitting parameter to analyze the *electric* nondipole effect in experimental data and compare the results to more sophisticated theoretical models. But in a first step, the parameter α is extracted from our CTSs for several scenarios that are summarized in Table I. It is evident that $\alpha \approx 1$ if the temporospatial dependence of the electric field is taken into account (scenarios V and W in Table I). In particular, the magnetic field does not significantly change the value of α.

The shearing of the momentum distribution which is induced by the *electric* nondipole effect is quantified by the value of α. The key point of the present Letter is to show this shearing in an experiment and in numerical *ab initio* simulations of the TDSE (time-dependent Schrödinger equation).

The experiment was performed using the same specialized COLTRIMS reaction microscope [27] and the same laser setup as in Ref. [24] (also see Supplemental Material [28]). The 25-fs laser pulses with a central wavelength of 800 nm and a repetition rate of 10 kHz are split into two counter-propagating pathways A and B. In pathway A (B) the light propagation-direction is parallel (antiparallel) to p_x and thus the light's wave vector k_{ph} is positive (negative). In both pathways lambda-quarter and lambda-half wave plates ensure that the laser pulses that enter the vacuum chamber are circularly polarized. The two pulses are focused from opposite sides to the same spot in the xenon-gas jet. Shutters in pathways A and B toggled between using the two possible pathways. This procedure allows us to eliminate most systematical errors which is essential, since the expected changes of the radius of the donut are on the order of 0.001 a.u.

Figure 2(a) shows the measured electron momentum distribution in cylindrical coordinates after integration over the angle in the polarization plane [see Figs. 1(a) and 1(b)]. Here, the intensity of the laser pulses in the focus is 8.1×10^{13} W/cm^2 (peak electric field of 0.034 a.u.). Figure 2(c) shows the same data as Fig. 2(a) after restricting the momenta to 0.5 a.u. $< p_r <$ 1.1 a.u. The forward shift of the electrons with 0.5 a.u. $< p_r <$ 1.1 a.u. that is due to the magnetic field is not visible in Fig. 2(c) because it is only $\langle p_x \rangle = 0.0021 \pm 0.0001$ a.u. (value has been determined by a Gaussian fit). This forward shift is due to the magnetic field and can be compared with the theoretically expected value $\langle p_x \rangle \approx p_r^2/(2c) + I_p/(3c) = 0.0027$ a.u. for $p_r = 0.68$ a.u. [24]. (The experimental uncertainty of $\langle p_x \rangle$ only takes the statistical error into account.)

From the data shown in Fig. 2(c), we have determined the most probable radial momentum using a Gaussian fit for every bin along p_x. The maximum of these Gaussian fits is shown by the black line and referred to as $\langle p_{r,A} \rangle$. The values of $\langle p_{r,A} \rangle$ as a function of p_x have a close to parabolic shape. In the next step the light propagation direction is inverted in the experiment and the analysis is done again and the result is referred to as $\langle p_{r,B} \rangle$. For each of the two resulting close to parabolic shapes the mean is subtracted using $\langle \tilde{p}_{r,A} \rangle(p_x) = \langle p_{r,A} \rangle(p_x) - q_A$ and $\langle \tilde{p}_{r,B} \rangle(p_x) = \langle p_{r,B} \rangle(p_x) - q_B$. Here, the scalar value q_A is the mean in p_r obtained from a Gaussian fit using the projection of the data shown in Fig. 2(c). q_B is the mean for pathway B in full analogy.

TABLE I. The parameter α at $p_x = 0$ a.u. is determined from the CTS model for various scenarios regarding the definition of the electromagnetic field [Eq. (2)] using a $\sin^2$ envelope with a total duration of 12 cycles.

Scenario	Light field's definition		ζ	χ	α
T	$\vec{E}(t)$,	No magnetic field	0	0	0.00
U	$\vec{E}(t)$,	$\vec{B}(t)$	0	1	0.00
V	$\vec{E}(\vec{x},t)$,	No magnetic field	1	0	1.07
W	$\vec{E}(\vec{x},t)$,	$\vec{B}(t)$	1	1	1.07

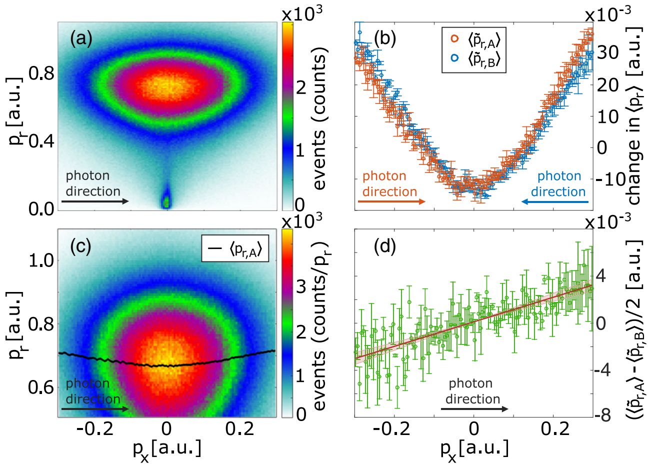

FIG. 2. Experiment on the strong-field ionization of xenon by circularly polarized light at a wavelength of 800 nm and an intensity of 8.1×10^{13} W/cm^2. (a) The electron momentum resolved on the momentum along the light propagation-direction, p_x, and the radial momentum in the plane of polarization, $p_r = \sqrt{p_y^2 + p_z^2}$, for a laser beam that has a propagation-direction as indicated ($k_{\rm ph} > 0$). (c) The same as (a) but zooming in and showing the most probable radial momentum, $\langle p_{r,A} \rangle$, as a function of p_x (black line). The red data points $\langle \tilde{p}_{r,A} \rangle$ in (b) show the same as the black line in (c) after subtracting a constant value (see text). The blue data points, $\langle \tilde{p}_{r,B} \rangle$, show the analogue to the red data points but for an inverted light propagation direction ($k_{\rm ph} < 0$). (d) $S(p_x) = [\langle \tilde{p}_{r,A} \rangle(p_x) - \langle \tilde{p}_{r,B} \rangle(p_x)]/2$ is shown in green. The red line is a linear fit to the green data points using α as a free parameter for $S(p_x) = \alpha (p_x/c) A_0$. The value of $\alpha A_0/\text{a.u.} = 1.43 \pm 0.23$ is obtained from the linear fit and is used as a figure of merit to describe the *electric* nondipole effect. The error bars show the standard deviation of the statistical errors.

The results for $\langle \tilde{p}_{r,A} \rangle$ and $\langle \tilde{p}_{r,B} \rangle$ are presented in Fig. 2(b). Within the dipole approximation the close to parabolic shape would be forward-backward symmetric and the p_x dependence would be caused by nonadiabatic effects and Coulomb interaction of the electron with its parent ion after tunneling [29]. To disentangle the symmetric contributions from the nondipole effects, the difference

$$S(p_x) = \frac{\langle \tilde{p}_{r,A} \rangle(p_x) - \langle \tilde{p}_{r,B} \rangle(p_x)}{2} \tag{4}$$

is shown in Fig. 2(d). The slope of $S(p_x) = \alpha A_0 p_x/c$ is found by fitting and we obtain a value of $\alpha = 2.38 \pm 0.38$ (which includes the statistical error only). We estimate the systematic error of α to be ± 0.42. As suggested by the illustration in Fig. 1(b), we find that $\langle p_r \rangle(p_x)$ linearly increases as a function of p_x for $k_{\rm ph} > 0$. Thus, the electrons flying in the forward direction show a larger radial momentum than those that are emitted into the backward direction. So qualitatively, the experimental findings are in line with the expectation from Eq. (3). We have repeated the experiment [28] using an intensity of 6.8×10^{13} W/cm^2 (1.2×10^{14} W/cm^2) and obtained $\alpha = 1.51 \pm 0.31$ ($\alpha = 3.10 \pm 0.10$) [32]. Thus, we find that the experimentally obtained value of α increases as a function of the light intensity [33].

For a quantitative comparison we have performed numerical simulations of the 3D TDSE including nondipole effects to first order in $1/c$ [14,24] and using an effective potential for xenon [34] converted into a pseudopotential for the $5p$ state at cutoff radius $r_{cl} = 2$ a.u. [35]. Based on the corresponding momentum distribution for a short laser pulse with sin^2-envelope of 3 cycles total duration, the value of α is obtained by a linear fit to $S_{\rm TDSE}(p_x) = [\langle p_r \rangle(p_x) - \langle p_r \rangle(-p_x)]/2$. The obtained values of α are shown in Fig. 3 for a wide range of intensities. The values of α are in the range from 0.75 to 0.78 and are systematically smaller than the naively expected value of $\alpha \approx 1$ [see Table I and Eq. (3)].

To deepen our understanding of the electric nondipole effect theoretically, we have also studied a quantum-orbit model derived from the strong-field approximation [12,17] (SFA) by application of a saddle-point approximation (analogous to the procedure in Ref. [24]). The resulting values of α are in good agreement with the TDSE result (see Fig. 3) [36]. In particular, this shows that the long-range ionic potential, which is not included in SFA, does not significantly influence the value of α. The most important difference comparing the SFA to the CTS model is that the SFA incorporates initial momentum offsets, i.e., the initial distribution of the freed electrons is not rotationally symmetric at the tunnel exit [29]. In first order of $1/c$ and leading order of the Keldysh parameter $\gamma = \sqrt{2I_p}/A_0$ the most probable momentum as a function of p_x is given by

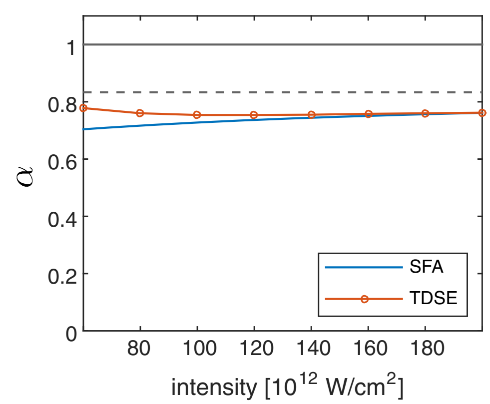

FIG. 3. Dependence of α at $p_x = 0$ a.u. on the intensity for a xenon atom at a wavelength of 800 nm that is obtained from a numerical solution of the TDSE (red line) and using the SFA (blue line). The adiabatic limit of $\alpha = 5/6$ (gray thick dotted line) and the estimate based on Eq. (3) (gray thick solid line) are shown as horizontal lines.

$$\langle p_r \rangle (p_x) = A_0 + \frac{1}{3A_0}\left(I_p + \frac{p_x'^2}{2}\right) + \frac{A_0}{c} p_x, \qquad (5)$$

with the shifted momentum $p_x' = p_x - (U_p + 2I_p/3)/c$ (for a light propagation direction that is parallel to p_x). The second quadratic term that is due to nonadiabatic offset momenta is centered around the global maximum of the momentum distribution. Using Eq. (5) it can be shown, that in the adiabatic limit ($\gamma \approx 0$) the slope of $\langle p_r \rangle (p_x)$ is characterized by $\alpha = 5/6$. However, on the other hand, taking only the magnetic field after tunneling into account ($\zeta = 0$, $\chi = 1$) the model predicts a value of $\alpha = -1/6$ which can be shown but does not follow directly from Eq. (5). Our simulation results show that the value of α does not change by more than 20% if an ellipticity of $\epsilon = 0.8$ is used or spin-orbit splitting or the magnetic quantum number of the electronic ground state is considered [28]. Possible explanations for the deviations comparing the results from the TDSE and the experiment are, e.g., multielectron effects, which are not included in the simulation or the approximation of the atomic potential by a pseudopotential.

In conclusion we have found that the temporospatial structure of the electric field, that has been so far neglected in the literature on tunnel ionization, alters the momenta of the electrons emitted in strong-field ionization and leads to an *electric* nondipole effect. Microscopically the *electric* nondipole effect can be explained by the time-dependent force that acts on the electron in the lab frame. This force is due to the laser field and has a higher frequency for electrons that are traveling antiparallel to the light propagation direction than for electrons that travel with the light wave. This change in effective frequency is analogous to the Doppler effect and affects the energy that is transferred to the electron. Thus, the forward-backward symmetry of electron emission in strong-field ionization is broken not only by the well-known *magnetic* nondipole effect but also by an *electric* nondipole effect. We expect that the electric nondipole effect will also have an impact on the energetic position of ATI peaks.

A. H. and K. F. acknowledge support by the German Academic Scholarship Foundation. The experimental work was supported by the DFG (German Research Foundation). K. L. acknowledges support by the Alexander von Humboldt Foundation. S. B., M. L., and S. E. acknowledge funding of the DFG through Priority Programme SPP 1840 QUTIF.

[*]lin@atom.uni-frankfurt.de
[†]doerner@atom.uni-frankfurt.de
[‡]eckart@atom.uni-frankfurt.de

[1] M. O. Krause, Photo-ionization of krypton between 300 and 1500 eV. Relative subshell cross sections and angular distributions of photoelectrons, Phys. Rev. **177**, 151 (1969).

[2] J. W. Cooper, Photoelectron-angular-distribution parameters for rare-gas subshells, Phys. Rev. A **47**, 1841 (1993).

[3] L. V. Keldysh, Ionization in the field of a strong electromagnetic wave, Sov. Phys. JETP **20**, 1307 (1965), http://www.jetp.ac.ru/cgi-bin/dn/e_020_05_1307.pdf.

[4] M. Klaiber, K. Z. Hatsagortsyan, and C. H. Keitel, Above-threshold ionization beyond the dipole approximation, Phys. Rev. A **71**, 033408 (2005).

[5] S. Grundmann, F. Trinter, A. W. Bray, S. Eckart, J. Rist, G. Kastirke, D. Metz, S. Klumpp, J. Viefhaus, L. Ph. H. Schmidt, J. B. Williams, R. Dörner, T. Jahnke, M. S. Schöffler, and A. S. Kheifets, Separating Dipole and Quadrupole Contributions to Single-Photon Double Ionization, Phys. Rev. Lett. **121**, 173003 (2018).

[6] M. Yu. Ivanov, M. Spanner, and O. Smirnova, Anatomy of strong field ionization, J. Mod. Opt. **52**, 165 (2005).

[7] A. Sommerfeld and G. Schur, Über den Photoeffekt in der K-Schale der Atome, insbesondere über die Voreilung der Photoelektronen, Ann. Phys. (Berlin) **396**, 409 (1930).

[8] M. J. Seaton, Momentum transfer in photo-ionization processes, J. Phys. B **28**, 3185 (1995).

[9] M. Førre and A. S. Simonsen, Nondipole ionization dynamics in atoms induced by intense xuv laser fields, Phys. Rev. A **90**, 053411 (2014).

[10] S. Grundmann, M. Kircher, I. Vela-Perez, G. Nalin, D. Trabert, N. Anders, N. Melzer, J. Rist, A. Pier, N. Strenger, J. Siebert, P. V. Demekhin, L. Ph. H. Schmidt, F. Trinter, M. S. Schöffler, T. Jahnke, and R. Dörner, Observation of Photoion Backward Emission in Photoionization of He and N_2, Phys. Rev. Lett. **124**, 233201 (2020).

[11] C. T. L. Smeenk, L. Arissian, B. Zhou, A. Mysyrowicz, D. M. Villeneuve, A. Staudte, and P. B. Corkum, Partitioning of the Linear Photon Momentum in Multiphoton Ionization, Phys. Rev. Lett. **106**, 193002 (2011).

[12] P.-L. He, D. Lao, and F. He, Strong Field Theories Beyond Dipole Approximations in Nonrelativistic Regimes, Phys. Rev. Lett. **118**, 163203 (2017).

[13] S. Chelkowski and A. D. Bandrauk, Photon-momentum transfer in molecular photoionization, Phys. Rev. A **97**, 053401 (2018).

[14] S. Brennecke and M. Lein, High-order above-threshold ionization beyond the electric dipole approximation: Dependence on the atomic and molecular structure, Phys. Rev. A **98**, 063414 (2018).

[15] N. Haram, R. T. Sang, and I. V. Litvinyuk, Transverse electron momentum distributions in strong-field ionization: Nondipole and coulomb focusing effects, J. Phys. B **53**, 154005 (2020).

[16] T. Katsouleas and W. B. Mori, Comment on 'Packet Spreading, Stabilization, and Localization in Superstrong Fields', Phys. Rev. Lett. **70**, 1561 (1993).

[17] M. W. Walser, C. H. Keitel, A. Scrinzi, and T. Brabec, High Harmonic Generation Beyond the Electric Dipole Approximation, Phys. Rev. Lett. **85**, 5082 (2000).

[18] M. Dammasch, M. Dörr, U. Eichmann, E. Lenz, and W. Sandner, Relativistic laser-field-drift suppression of nonsequential multiple ionization, Phys. Rev. A **64**, 061402(R) (2001).

[19] S. Palaniyappan, A. DiChiara, E. Chowdhury, A. Falkowski, G. Ongadi, E. L. Huskins, and B. C. Walker, Ultrastrong

Field Ionization of $Ne^{n+}(n \leq 8)$: Rescattering and the Role of the Magnetic Field, Phys. Rev. Lett. **94**, 243003 (2005).
[20] A. Emmanouilidou and T. Meltzer, Recollision as a probe of magnetic-field effects in nonsequential double ionization, Phys. Rev. A **95**, 033405 (2017).
[21] M. Klaiber, E. Yakaboylu, H. Bauke, K. Z. Hatsagortsyan, and C. H. Keitel, Under-the-Barrier Dynamics in Laser-Induced Relativistic Tunneling, Phys. Rev. Lett. **110**, 153004 (2013).
[22] S. Chelkowski, A. D. Bandrauk, and P. B. Corkum, Photon Momentum Sharing Between an Electron and an Ion in Photoionization: From One-Photon (Photoelectric Effect) to Multiphoton Absorption, Phys. Rev. Lett. **113**, 263005 (2014).
[23] S. Chelkowski, A. D. Bandrauk, and P. B. Corkum, Photon-momentum transfer in multiphoton ionization and in time-resolved holography with photoelectrons, Phys. Rev. A **92**, 051401(R) (2015).
[24] A. Hartung, S. Eckart, S. Brennecke, J. Rist, D. Trabert, K. Fehre, M. Richter, H. Sann, S. Zeller, K. Henrichs, G. Kastirke, J. Hoehl, A. Kalinin, M. S. Schöffler, T. Jahnke, L. Ph. H. Schmidt, M. Lein, M. Kunitski, and R. Dörner, Magnetic fields alter strong-field ionization, Nat. Phys. **15**, 1222 (2019).
[25] CTSs with Coulomb interaction are sensitive to the choice of the tunnel exit position [37]. CTSs using tunnel exit positions that take non-adiabaticity and nondipole effects into account are beyond the scope of the current work.
[26] N. I. Shvetsov-Shilovski, M. Lein, L. B. Madsen, E. Räsänen, C. Lemell, J. Burgdörfer, D. G. Arbó, and K. Tőkési, Semiclassical two-step model for strong-field ionization, Phys. Rev. A **94**, 013415 (2016).
[27] J. Ullrich, R. Moshammer, A. Dorn, R. Dörner, L. Ph. H. Schmidt, and H. Schmidt-Böcking, Recoil-ion and electron momentum spectroscopy: Reaction-microscopes, Rep. Prog. Phys. **66**, 1463 (2003).
[28] See Supplemental Material at http://link.aps.org/supplemental/10.1103/PhysRevLett.126.053202 that provides additional details about the experiment. Moreover, the achieved resolution in the experiment is compared to the theoretical expectation, and theoretical details regarding the magnetic sub-levels in the initial state are discussed. The Supplemental Material includes the Refs. [29–31].
[29] S. Eckart, K. Fehre, N. Eicke, A. Hartung, J. Rist, D. Trabert, N. Strenger, A. Pier, L. Ph. H. Schmidt, T. Jahnke, M. S. Schöffler, M. Lein, M. Kunitski, and R. Dörner, Direct Experimental Access to the Nonadiabatic Initial Momentum Offset Upon Tunnel Ionization, Phys. Rev. Lett. **121**, 163202 (2018).
[30] O. Jagutzki, A. Cerezo, A. Czasch, R. Dörner, M. Hattas, M. Huang, V. Mergel, U. Spillmann, K. Ullmann-Pfleger, T. Weber, H. Schmidt-Böcking, and G. D. W. Smith, Multiple hit readout of a microchannel plate detector with a three-layer delay-line anode, IEEE Trans. Nucl. Sci. **49**, 2477 (2002).
[31] D. G. Altman and J. M. Bland, Standard deviations and standard errors, Br. Med. J. **331**, 903 (2005).
[32] Analysis of another data set for the strong field ionization of argon using circularly polarized light at 800 nm yields a value of $\alpha = (1.315 \pm 0.485)/(A_0/\mathrm{a.u.}) = 1.69 \pm 0.62$ using $A_0 = 0.78$ a.u. (see Fig. 6.57 in Ref. [38]).
[33] In order to judge if saturation is relevant in the experiment, we have analyzed the changes of $\langle p_r \rangle$ as a function of the laser intensity. We found that for our 25-fs laser pulses with a central wavelength of 800 nm the single ionization of xenon is saturated [not saturated] for an intensity of $1.2 \times 10^{14}\ \mathrm{W/cm^2}$ [$6.8 \times 10^{13}\ \mathrm{W/cm^2}$]. This is consistent with Ref. [39] where the saturation intensity of xenon was found to be $7 \times 10^{13}\ \mathrm{W/cm^2}$ using 100-fs laser pulses with a central wavelength of 620 nm.
[34] X. M. Tong and C. D. Lin, Empirical formula for static field ionization rates of atoms and molecules by lasers in the barrier-suppression regime, J. Phys. B **38**, 2593 (2005).
[35] N. Troullier and J. L. Martins, Efficient pseudopotentials for plane-wave calculations, Phys. Rev. B **43**, 1993 (1991).
[36] In principle, more general approaches could be considered for the quantum orbit model [40].
[37] H. Ni, U. Saalmann, and J.-M. Rost, Tunneling exit characteristics from classical backpropagation of an ionized electron wave packet, Phys. Rev. A **97**, 013426 (2018).
[38] A. Hartung, Der Photonenimpuls in der Starkfeldionisation, Ph.D. thesis, Goethe University Frankfurt, Frankfurt am Main, Germany, 2019.
[39] L. F. DiMauro, P. Agostini, B. Bederson, and H. Walther, Ionization dynamics in strong laser fields, Adv. At. Mol. Opt. Phys. **35**, 79 (1995).
[40] D. B. Milošević, S. Hu, and W. Becker, Quantum-mechanical model for ultrahigh-order harmonic generation in the moderately relativistic regime, Phys. Rev. A **63**, 011403(R) (2000).